Optimised Electro-Osmotic Flow in Rectangular Microchannels with Smoothed Corners

Optimised Electro-Osmotic Flow in Rectangular Microchannels with Smoothed Corners

Marco Lorenzini[1],**Nicola Suzzi**[2]

[1] Università di Bologna, DIN – Dipartimento di Ingegneria Industriale, Via Fontanelle 40, I-47121, Forlì (FC), Italy
[2] Università di Udine, DPIA - Dipartimento Politecnico di Ingegneria e Architettura, Via delle Scienze 206 - I-33100 Udine (UD), Italy

E-mail: marco.lorenzini@unibo.it

Abstract. Electro-osmotic flows are a means of circulating polar fluids through microchannels without resorting to mechanical pumping. The lack of moving parts, of noise and the ease of integration in silicon chips make them an interesting option for microchip cooling and miniaturized total analysis systems. This paper describes an optimization in terms of first- and second-law analysis of the cross-section of a microchannel subject to electro-osmotic flow. Starting from rectangular cross-sections of different aspect ratios, its corners are progressively smoothed and the resulting Poiseuille and Nusselt numbers computed. Performance evaluation criteria are then used to assess the change in, among others, heat transfer rate, temperature difference between wall and bulk fluid, and equivalent pumping power. The entropy number is also computed and the results commented. It is found that the latter criterion highlights a configuration of minimum entropy generation, whereas the trends of the heat transfer and temperature difference are opposite to that of the equivalent pumping power.

1. Introduction

Practical applications of micro-flow devices (MFDs) are growing in number and the future outlook appears promising, yet MFDs are still the subject of much fundamental research, [1]. Among MFDs, microchannel heat sinks can remove high heat flux densities, but pressure drop across the channels, particularly when liquids are employed, can be a crippling drawback. When charged surfaces are involved, electro-osmosis can be used, since it allows motion of a liquid relative to a charged surface under the action of an electric field, [2], without the need for moving parts. Also, the system lends itself to being realized directly onto electronic chips, [3], and micro total analysis systems (μ- TAS), [4]. Performance of a microchannel heat sink can be improved by modifying the shape of its cross-section, optimising it according to a chosen set of constraints, [5, 6]. In spite of their great applicative potential where removal of high heat fluxes is in demand, the related pressure drop may be significant, especially when liquids are employed as coolants, with the reduction in hydraulic diameter of the ducts quickly leading to viscous heating of the fluid circulated, [7, 8], which reverses the direction of the heat flow. At small scales, however, flow devices can exploit micro-effects, [7], such as electro-osmosis, which allows the motion of a liquid relative to a charged surface, induced by an applied external potential gradient across a microchannel, [2, 9]. If a polar fluid is used in combination with channel walls possessing a net electrical charge, an inhomogeneous charge distribution develops in the liquid,

which can be moved by applying electric field over the length of the channel, which acts on the layer of mobile ions close to the walls: the flow which originates is called electro-osmotic (EOF). EOF devices have several advantages: they do not have moving parts, are therefore free of noise and vibrations and no lubrication is needed. Also, liquid reservoirs require tiny volumes, making them ideal for direct connection to the chips. EOFs have been reported to yield experimental Nusselt numbers about 10% larger than pressure-driven flow (PDF) for the same geometry, although Joule heating may become significant when the applied voltage between the electrodes increases beyond a certain threshold, [10]. Voltage signals sent to electrodes make implementation of EOF devices easier than manufacturing and controlling a micro mechanical pump. Among the drawbacks, the chemical composition at the interface can significantly alter the velocity profiles, which are markedly different from those exhibited by pressure-driven flows, and Joule heating in the fluid may partly or completely offset its cooling action, [2]. Electro-osmotic flows in microchannels have been the subject of several fundamental investigations, for a variety of cross-section, ranging from the common circular ducts and parallel plates, [11], to unusual geometries such as polygonal, elliptical and triangular ducts, [3, 12, 13], as has been the use of electro-osmotic pumps (EOPs), [14, 15], sometimes with the specific purpose of electronics cooling, [10, 16, 17]. The use of non-Newtonian fluids, [18, 19], and nanofluids, [20], is also a recent field of investigation.

For the single microchannel, one of the earliest works is that of Rice and Whitehead, [11], who dropped the assumption of negligible EDL thickness as in the classical treatment by Smoluchowski, and predicted an electro-viscous effect, i.e. a maximum in the apparent viscosity of the flow. Maynes and Webb, [21], investigated the convective heat transfer associated to purely electro-osmotic and both pressure and electro-osmotically driven flows for fully developed flow in circular ducts and parallel plate channels, [22], assuming that the Debye length reached to half-width Z of the channel. Their findings demonstrated that the factors with the strongest influence on the temperature profile and Nusselt number are Z, the intensity of the non-dimensional Joule heating and the ratio of the external electric field to pressure gradient.

Vocale et al., [13], focussed their investigations on triangular microchannels both with and without superimposed pressure gradient. The velocity field was found to be strongly influenced by the aspect ratio and the electro-kinetic diameter of the channel. The role of the relative ratio of pressure forces and electrical forces acting on the fluid was also analysed and characteristic curves for EOPs with triangular channels were obtained.

The discussion above reveals how research on electro-osmotic flow in microchannels has been very active in the recent past, touching a variety of subjects such as the fluids employed, the electric field magnitude, the presence of the pressure gradient, and the shape of cross-section which can take several forms (circular, trapezoidal, rectangular, etc.) thanks to the current development of micro-fabrication technologies. Optimisation of the cross-section can lead to improved performance in terms of increased heat transfer and decreased pressure drop and entropy production, and this can be achieved through smoothing of its corners, as demonstrated in [23, 24]. Investigation has been extended to pressure-driven flows in microchannels with and without viscous dissipation, [8], and to electro-osmotic flows in the fully developed and constant heat flux and perimeter temperature case, [25], employing the results to carry out a first-law analysis based on performance evaluation criteria (PECs), a method detailed in e.g. [5], which is based on a first-law approach. This work investigates numerically the performance of a microchannel subject to EOF and with uniform wall temperature when its base, rectangular, cross-section has its corner progressively smoothed, keeping the thermal entry region into account, thus solving a so-called Graetz problem. Optimisation is carried out using PECs and entropy generation minimisation, [6], to account for both the first and second law of thermodynamics, as already proposed by [26]. The investigation is similar to what was done in [25] for uniform heat flux and temperature over the cross-section and fully-developed flow. The

factors influencing the thermal behaviour of the microchannel are investigated and an analysis of the influence of Joule heating to heat transfer ratio is also given. The practical uses of the results are highlighted, as their usefulness in conducting PEC-type analyses.

2. Problem modelling and method of solutions

The geometry investigated is plotted in Fig. 1, which shows the cross-section a × b in dimensions, with smoothed corners of radius of curvature r, Fig. 1(a), and the channel of length L, Fig. 1(b), with its axis along the L direction of a reference frame. To obtain the Poiseuille and Nusselt numbers, Po and Nu, needed for optimisation, the electric potential, velocity and temperature fields must be computed. The corresponding governing equations with suitable boundary conditions are written in the following directly in non-dimensional form; for a detailed description of how the equations are obtained using the Gouy-Chapman model, [2], see e.g. [25, 27].

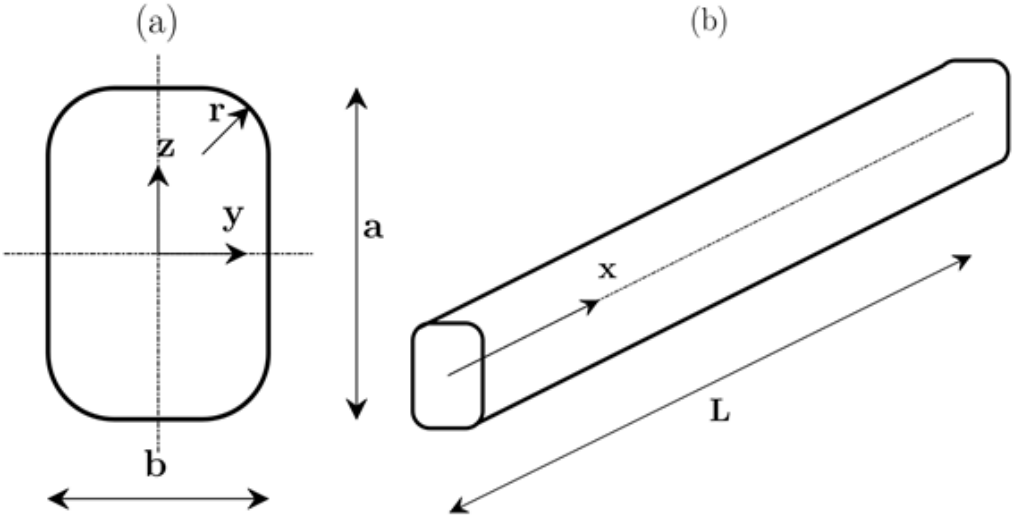

Figure 1: Cross-section (a) and channel (b).

2.1. Electric potential

The non-dimensional formulation of the equation for the electric potential distribution,Ψ is,

$$\frac{\partial^2 \Psi}{\partial Y^2} + \frac{\partial^2 \Psi}{\partial Z^2} = (k_D \, D_h)^2 \, \sinh \Psi \tag{1}$$

D_h is the hydraulic diameter and k_D is the Debye–Hückel parameter (m^{-1}), [2, 7], and represents the inverse of characteristic length (Debye length) for the electric double layer (EDL). The non-dimensional value, Ψ_0, of the potential at the Stern plane which separates the two layers forming the EDL is used as a boundary condition over the non-dimensional perimeter, $\partial\Omega$:

$$\Psi|_{\partial\Omega} = \Psi_0 \tag{2}$$

2.2. Velocity field

A steady, hydrodynamically developed laminar flow of a Newtonian, incompressible fluid with uniform thermophysical properties through a microchannel of uniform cross section is considered.

The non-dimensional governing equation for the only non-zero component of the velocity U is thus:

$$\frac{\partial^2 U}{\partial Y^2} + \frac{\partial^2 U}{\partial Z^2} = \tilde{E} \sinh \Psi \tag{3}$$

where $\tilde{\mathrm{E}}$ is the non-dimensional external electric field. The no-slip boundary condition is imposed through the solid wall, $\mathrm{U}|_{\partial\Omega} = 0$. Knowledge of the velocity field allows computation of Po, [28].

2.3. Temperature field

The non-dimensional temperature distribution $\Theta(\mathrm{X}, \mathrm{Y}, \mathrm{Z})$ is obtained from the solution of the non-dimensional energy equation below,

$$\mathrm{Re}\,\mathrm{Pr}\,\frac{U}{U_b}\,\frac{\partial \Theta}{\partial X} = \frac{\partial^2 \Theta}{\partial Y^2} + \frac{\partial^2 \Theta}{\partial Z^2} + M_z \tag{4}$$

Pr is the Prandtl number of the fluid, while $\mathrm{U_b}$ and Re are the non-dimensional bulk velocity and the Reynolds number. The parameter $\mathrm{M_z}$ appearing in Eq. (4) is defined as

$$M_z = \frac{\sigma\ (D_h\, E_x)^2}{\lambda\ (T_w - T_i)} \tag{5}$$

σ and λ are the fluid's electrical resistivity and thermal conductivity, $\mathrm{E_x}$ is the electric field applied at the ends of the channel, and $\mathrm{T_w}$ and $\mathrm{T_i}$ the wall temperature and the fluid temperature at the inlet respectively. $\mathrm{M_z}$ relates Joule heating within the fluid to the heat transfer at the wall, and its role is similar to that of the Brinkman number in pressure-driven flows with significant viscous dissipation, [8, 29] A uniform wall temperature is imposed, and a uniform temperature profile at the channel entrance ($\mathrm{X_0} = 0$) is chosen, so that

$$\Theta|_{\partial\Omega} = 0,\ \Theta(Y, Z)|_{X_0} = 1 \tag{6}$$

As discussed in [27], use of a preparation length, [30], to account for Joule heating within the fluid is not necessary in this case.

2.4. Numerical modelling

The numerical solution of Eqs. (1), (3) and (4) was obtained using the open source software `GNU Octave` and a number of additional libraries, as detailed in [27]. The electric potential and velocity fields are solved sequentially over the two-dimensional domain corresponding to the cross-section; this would not appear possible for the energy equation, Eq. (4), yet it has the form of a parabolic partial differential equation, so the three-dimensional physical problem can be reduced to a two-dimensional mathematical problem. Implementing the $\theta-$weighted scheme for marching over channel axis, Eq. (4) is discretised as if it were a two-dimensional, unsteady problem, in the form

$$\mathrm{Re}\,\mathrm{Pr}\,\frac{U}{U_b}\left[\frac{\Theta}{\Delta X}\right]^{n+1} - \theta\left[\frac{\partial^2 \Theta}{\partial Y^2} + \frac{\partial^2 \Theta}{\partial Z^2}\right]^{n+1} = \mathrm{Re}\,\mathrm{Pr}\,\frac{U}{U_b}\left[\frac{\Theta}{\Delta X}\right]^{n} + (1-\theta)\left[\frac{\partial^2 \Theta}{\partial Y^2} + \frac{\partial^2 \Theta}{\partial Z^2}\right]^{n} + M_z \tag{7}$$

where n denotes the integration step along the channel axis.

2.5. Entropy generation

Entropy generation is obtained in non-dimensional form by writing the entropy balance over a length dx of the channel and integrating it between entrance and exit, see e.g. [26]. Knowledge of the temperature and velocity fields allows computation of the entropy generation number $\mathrm{N_S}$, [6], which is the ratio of the total entropy production in a tentative configuration (i.e. for a given smoothing radius) to the reference one (i.e. with sharp corners). $\mathrm{N_S}$ can be written as a function of two contributions, one, $\mathrm{N_T}$, due to heat transfer, which includes Joule heating, and one, $\mathrm{N_P}$, due to the driving force, and of their ratio $\Phi_\mathrm{r} = \mathrm{N_P}/\mathrm{N_T}$:

$$N_S = \frac{N_T + \Phi_r N_P}{1 + \Phi_r} \tag{8}$$

The two contributions $\mathrm{N_T}$ and $\mathrm{N_P}$ can be written as

$$N_T = \frac{\dot{Q}}{\dot{Q}_r}\left[\frac{T_{b_{i_r}}}{T_{b_{o_r}}} + \frac{\dot{Q}/\dot{Q}_r}{\dot{m}/\dot{m}_r}\left(1 - \frac{T_{b_{i_r}}}{T_{b_{o_r}}}\right)\right]^{-1} \frac{(T_{b_i} - T_w)}{(T_{b_i} - T_w)_r} \cdot \exp\left[4 \cdot St_r \frac{L_r}{D_{h_r}}\left(1 - \frac{St}{St_r}\frac{L/L_r}{D_h/D_{h_r}}\right)\right] \tag{9}$$

$$N_P = \frac{P}{P_r} = \frac{\left(\dot{m}/\dot{m}_r\right)^2 Po/Po_r \cdot L/L_r}{\Omega/\Omega_r D_h/D_{h_r}} = P' \tag{10}$$

the subscript r denotes quantities in the reference configuration, i is for 'inlet', o for 'outlet' and b for 'bulk'; the superscript $'$ is used for the ratio of a quantity to its value in the reference configuration. The heat flux is $\dot{\mathrm{Q}}$, $\dot{\mathrm{m}}$ is the mass flowrate and St is the Stanton number $\mathrm{St} = \mathrm{Nu}/\left(\mathrm{Re} \cdot \mathrm{Pr}\right)$. Since the fluid properties are assumed to be constant, $\mathrm{St}' = \mathrm{Nu}'/\mathrm{Re}'$.

3. Results and discussion

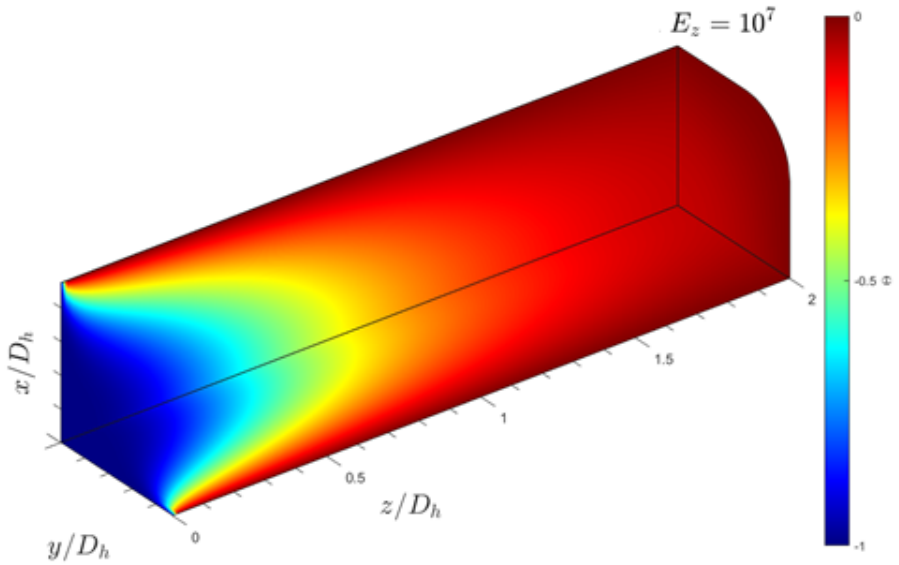

Figure 2: Temperature field along the channel.

The code was verified with the analytical and numerical results in [31] and [25] respectively, and validated with the experimental results of [10], and was then employed to determine the

velocity and temperature distribution under the same conditions as in [27] for four values of the aspect ratio, $\beta = 1, 0.50, 0.25, 0.10$ and a non-dimensional radius of curvature $0 \leq \mathrm{R_c} \leq 1$; since one further geometrical constraint must be added to apply PEC optimisation [25], it was chosen to keep the hydraulic diameter unchanged, $\mathrm{D'_h} = 1$. To compute $\mathrm{N_S}$, $\mathrm{N_T}$ and $\mathrm{N_P}$,the relative entropy generation in the reference condition was chosen as $\Phi_\mathrm{r} = 0.1$, a reasonable estimate, see e.g. [23] for details, and $\mathrm{T_{b_{ir}}}/\mathrm{T_{b_{or}}} = 0.95$, the latter corresponding to an inlet temperature $\mathrm{T_{b_{ir}}} = 298\,\mathrm{K}$ and a temperature increase of 15 K between inlet and outlet.

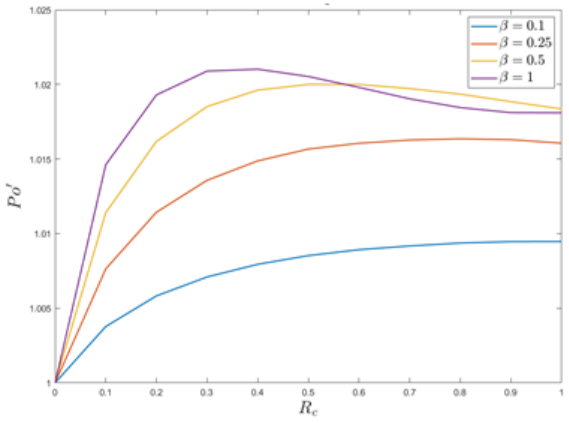

Figure 3: Relative Poiseuille number.

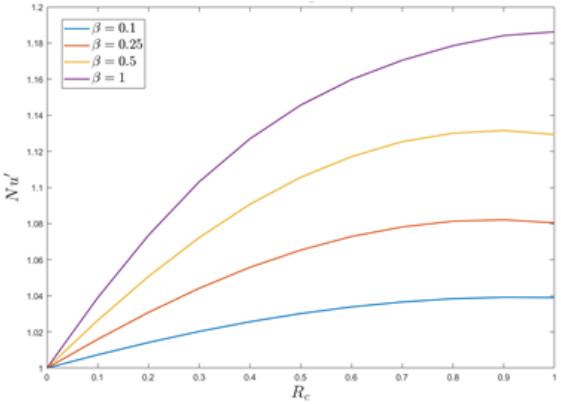

Figure 4: Relative Nusselt number.

A typical temperature profile is shown in Fig. 2, for one quarter of the channel (thanks to the problem's symmetries); the thermal entry region is easily discernible.

From the velocity and temperature distribution, Po and Nu were computed according to [27, 28] and expressed as third order polynomials in the β and $\mathrm{R_c}$, whose coefficients are given in [27]. The relative values of the two quantities $\mathrm{Po'}$ and $\mathrm{Nu'}$, which are needed for PEC optimisation are easily obtained from the above data and are plotted in Fig. 3 and Fig. 4 respectively. It can be noticed that $\mathrm{Nu'}$ increases with $\mathrm{R_c}$ and reaches a rather flat maximum for the intermediate values of β at high radii of curvature, $\mathrm{Po'}$ has a maximum for $\beta = 1, 0.5, 0.25$ and a relative minimum for $\beta = 1$, $\mathrm{R_c} = 0.9$. This testifies that smoothing the corners increases the transport phenomena, with benefits to heat transfer and penalties for pumping power, yet, for larger aspect ratios, where the curved stretches take up a significant length of the sides, maximum increase in heat transfer does not necessarily correspond to the maximum frictional losses.

3.1. Performance evaluation criteria and related entropy production: FG1a

Due to space constraints, only maximisation of heat transfer under fixed mass flowrate, channel length and temperature difference between wall and bulk fluid at the inlet is shown and discussed. This PEC is known as FG1a. Under these conditions, the objective function for $\dot{\mathrm{Q}}'$ becomes:

$$\dot{Q}' = \frac{1 - \exp\left(-4St_r \frac{L_r}{D_h} \left(\frac{St'}{Dh'} \right) \right)}{1 - \exp\left(-4St_r \frac{L_r}{D_{h_r}} \right)} \tag{11}$$

with $\mathrm{Pr} = 7$, $\mathrm{L_r} = 1\,\mathrm{cm}$, $\mathrm{D_{h_r}} = 3\,\mu\mathrm{m}$ and, as mentioned, $\mathrm{D'_h} = 1$. The trend of $\dot{\mathrm{Q}}'$ is shown in Fig. 5 and is similar to that of $\mathrm{Nu'}$.

The pumping power under the FG1a constraints is closely related to M_z, in fact

$$P' = \sqrt{M_z'} = Po'/\Omega' \tag{12}$$

Since M_z is closely related to the external electric field, which is responsible for fluid motion in EOF, it is the trend of M_z' which is reported in Fig. 6. Again, pumping power increases with the radius of curvature, and the change is steeper, the larger the aspect ratio.

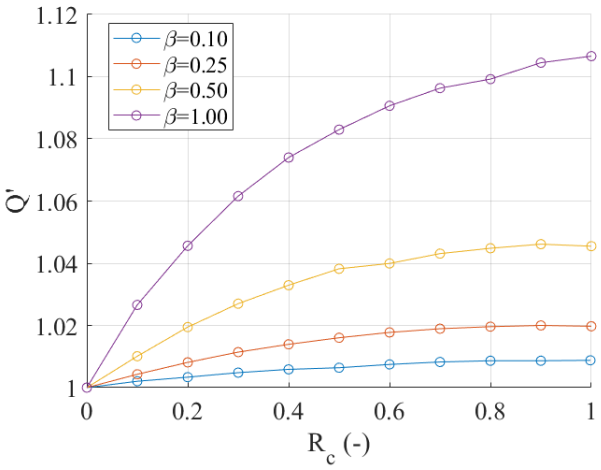

Figure 5: Relative heat flux, criterion FG1a.

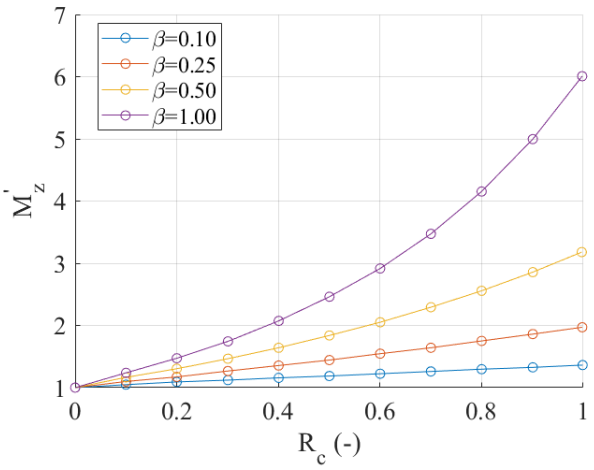

Figure 6: M_z', criterion FG1a.

If the PECs alone are considered, the trends of heat transfer and pumping power are conflicting, so it is not clear which configuration would yield the best results; second-law analysis can supply some further insight. The results for N_T and N_P are plotted in Figs. 7 and 8, and the resulting entropy generation number, N_S in Fig. 9.

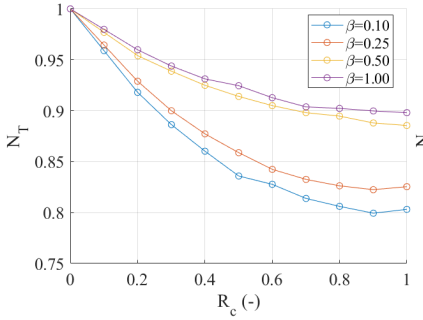

Figure 7: Entropy number for temperature, criterion FG1a.

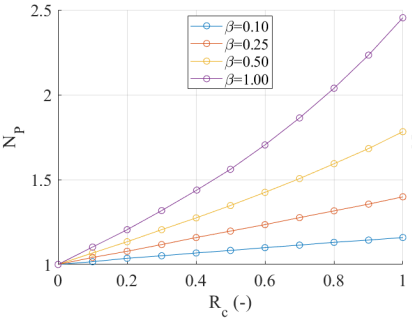

Figure 8: Entropy number for pressure, criterion FG1a.

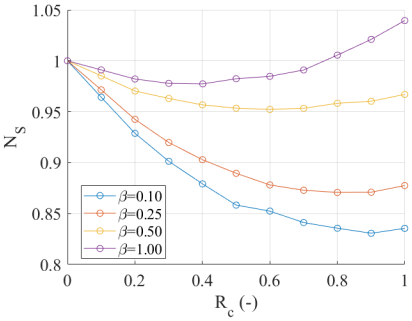

Figure 9: Entropy generation number, criterion FG1a.

It can be seen clearly that entropy generations due to heat transfer and frictional losses have opposing trends: entropy generation is always lower for sections with smoothed corners, as compared to sharp corners, and the smaller aspect ratios also exhibit a minimum, whilst the entropy generation due to pumping losses is always increasing with the radius of curvature and with the aspect ratio. The total entropy generation, which is represented by N_S, exhibits a minimum for all aspect ratios considered, at increasing values of the radius of curvature, the

larger β is. Also, for $\beta = 1$ N_S exceeds unity, i.e. is larger than in the reference configuration, for $\beta \geq 0.8$, and is about $N_S \approx 0.97$ at its minimum, hinting at almost no changes in the entropy generated (but with an increase in the heat flux of over 10% at large R_c, see Fig. 5). When the aspect ratio is low, on the contrary, a decrease of almost 20% in entropy production can be achieved, yet a minimal increase at best in the heat transfer can be expected.

4. Conclusions

In this work, the Graetz problem is solved for the electro-osmotic flow in a microchannel with uniform wall temperature, with a rectangular cross-section and rounded corners. Velocity and temperature fields have been used to compute the Poiseuille, Nusselt and the entropy generation numbers for the evaluation of the microchannel performance according to both PEC and entropy minimisation. It is found that the heat transfer increases with the radius of curvature, with a rather flat maximum for high R_c's, whereas the increase in pumping power, as represented by M_z is much steeper, and in both cases the results increase with the aspect ratio. Entropy generation increases steadily with both the radius of curvature and the aspect ratio when friction losses are involved, whilst the heat transfer has a decreasing entropy production with the increase of the radius of curvature and the decrease of the aspect ratio. The entropy generation number shows that there is a minimum in generated entropy for every aspect ratio, and that the decrease is larger for smaller aspect ratios. The method is of general validity and can therefore be applied to other values of the parameter involved and to other PECs.

Nomenclature

D_h	Hydraulic diameter	m
$\tilde{E}$	Nondimensional electric field	-
k_D	Debye–Hückel parameter	m^{-1}
L	Channel length	m
M_z	Joule heating to heat transfer ratio, Eq.(5)	-
N_P	Contribution of pressure drop to entropy generation number, Eq.(10)	-
N_T	Contribution of heat transfer to entropy generation number, Eq.(9)	-
N_S	Entropy generation number, Eq.(8)	-
P	Pumping power	W
Po	Poiseuille number	-
Pr	Prandtl number	-
$\dot{Q}$	Thermal power	W
R	Nondimensional radial coordinate	-
Re	Reynolds number	-
St	Stanton number	-
T	Temperature	K
U	Nondimensional velocity	-
x	Axial coordinate	m
X	Nondimensional x-coordinate	-
Y	Nondimensional y-coordinate	-
Z	Nondimensional z-coordinate	-

Greek letters		
β	Aspect ratio of the channel	-
γ	Nondimensional smoothing radius	-
$\partial\Omega$	Nondimensional perimeter	-
λ	Thermal conductivity	$\mathrm{W{\cdot}m^{-1}{\cdot}K^{-1}}$
μ	Fluid viscosity	Pa·s
Phi	Ratio of N_P to N_T	
Ψ	Nondimensional electric potential	-
Ψ_0	Nondimensional Stern potential	-
σ	Electric conductivity	$\mathrm{S{\cdot}m^{-1}}$
Θ	Nondimensional temperature	K
Subscripts and superscripts		
b	Bulk	
c	Curvature	
i	Inlet	
o	Outlet	
r	Reference	
th	Thermal	
w	Wall	
x	Component along the x-direction	

References

[1] Han Y, Liu Y and Li Mand Huang J 2012 *Energy Procedia* **14** 148–153
[2] Kirby C 2010 *Micro- and Nanoscale Fluid Mechanics* (Cambridge, UK: CUP)
[3] Ohadi M, Choo K, Dessiatoun S and Cetegen E 2013 *Next Generation Microch. Heat Exch.* (NY: Springer)
[4] Tabeling P 2010 *Introduction to microfluidics* (Oxford, UK: Oxford University Press)
[5] R L Webb 1994 *Principles of Enhanced Heat Transfer* (New York: Wiley)
[6] A Bejan 1982 *Entropy generation through heat and fluid flow* (New York: Wiley)
[7] Bruus H 2010 *Theoretical microfluidics* (Oxford: OUP)
[8] Lorenzini M and Morini G 2011 *Heat Transfer Engineering* **32** 1108–1116
[9] Hossan M, Dutta D, Islam N and Dutta P 2018 *Electrophoresis* **39** 702–731
[10] Al-Rjoub M, Roy A, Ganguli S and Banerjee R 2011 *Int. Journal of Heat and Mass Tr.* **54** 4560–4569
[11] Rice C and Whitehead R 1965 *Journal of Physical Chemistry* **69** 4017–4024
[12] Wang C Y and Chang C C 2011 *Electrophoresis* **32** 1268–1272
[13] Vocale P, Geri M, Morini G and Spiga M 2014 *Journal of Physics: Conference Series* **501**
[14] Geri M, Lorenzini M and Morini G 2012 *International Journal of Thermal Sciences* **55** 114–121
[15] Al-Rjoub M, Roy A, Ganguli S and Banerjee R 2015 *Journal of Electronic Packaging, Trans. ASME* **137**
[16] Al-Rjoub M, Roy A, Ganguli S and Banerjee R 2012 *ASME 2012 3rd International Conference on Micro/Nanoscale Heat and Mass Transfer, MNHMT 2012* 829–833
[17] Pramod K and Sen A 2014 *Journal of Electronic Packaging, Trans. ASME* **136** 03101201–03201214
[18] Shamshiri M, Khazaeli R, Ashrafizaadeh M and Mortazavi S 2012 *J. of Non-Newt. Fl. Mech.* **173-174** 1–12
[19] Shit G, Mondal A, Sinha A and Kundu P 2016 *Physica A: Statist. Mech. and its Applications* **462** 1040–1057
[20] Al-Rjoub M, Roy A, Ganguli S and Banerjee R 2015 *Int. Comm. in Heat and Mass Transfer* **68** 228–235
[21] Maynes D and Webb B 2003 *International Journal of Heat and Mass Transfer* **46** 1359–1369
[22] Maynes D and Webb B 2003 *Journal of Heat Transfer* **125** 889–895
[23] Ray S and Misra D 2010 *International Journal of Thermal Sciences* **49** 1763–1775
[24] Chakraborty S and Ray S 2011 *International Journal of Thermal Sciences* **50** 2522–2535
[25] Lorenzini M 2020 *Thermal Science and Engineering Progress* **19**
[26] Zimparov V 2000 *International Journal of Heat and Mass Transfer* **43** 3137–3155
[27] Suzzi N and Lorenzini M 2021 *Fluids* **6**
[28] Morini G, Lorenzini M, Salvigni S and Spiga M 2006 *International Journal of Thermal Sciences* **45** 955
[29] Lorenzini M, Daprá I and Scarpi G 2017 *Applied Thermal Engineering* **122** 118–125
[30] Suzzi N and Lorenzini M 2019 *International Journal of Thermal Sciences* **145** 10603201–10603210
[31] Y Jian, L Yang and Q Liu 2010 *Phys. Fluids* **22** 042001